Supporting Information

Phase Transformations of Individual Ti_3O_5 Nanocrystals Studied by *In-Situ* Electron Microscopy

Yaowei Hu[1 a], Hilaire Mba[1 a], Matthieu Picher[1], Hiroko Tokoro[2]*, Shin-ichi Ohkoshi[3], Céline Mariette[4], Ritwika Mandal[5], Maryam Alashoor[5], Philippe Rabiller[5]*, Maciej Lorenc[5], and Florian Banhart[1]*

[1)] Institut de Physique et Chimie des Matériaux, UMR 7504, Université de Strasbourg, CNRS, 67034 Strasbourg, France

[2)] Department of Materials Science, Institute of Pure and Applied Sciences, University of Tsukuba, Tsukuba, Ibaraki, Japan

[3)] Department of Chemistry, School of Science, The University of Tokyo, Bunkyo-ku, Tokyo, Japan

[4)] ESRF - The European Synchrotron, Grenoble, France

[a] These authors contributed equally to this work

* tokoro@ims.tsukuba.ac.jp

* philippe.rabiller@univ-rennes.fr

* florian.banhart@ipcms.unistra.fr

1. Setup of the electron microscope

The TEM is based on an utrafast or dynamic transmission electron microscope where lasers are used for exciting the specimen and creating photoelectron pulses. In this study, a continuous electron beam from a thermal cathode was used for imaging and diffraction. Laser pulses are only needed for triggering the phase transformation in the specimen. The laser beam enters the column of the microscope through a window and is reflected by an annular mirror onto the specimen as shown in Fig. S1 below. The laser power was measured in front of the entrance window of the microscope column. The laser was focused by a lens outside the column so that a spot of approximately 150 µm in diameter was achieved on the specimen. For centering the laser on the specimen, a test specimen was used where gold particles on a carbon film transform and coalesce under laser irradiation. Single 7 ns pulses at 1064 nm are used for inducing the phase transition. For the continuous heating of the specimens, a standard heating stage (Gatan, single tilt) with resistive heating was used. For more details about the microscope, see M. Picher et al., *Ultramicroscopy* **2018**, *188*, 41.

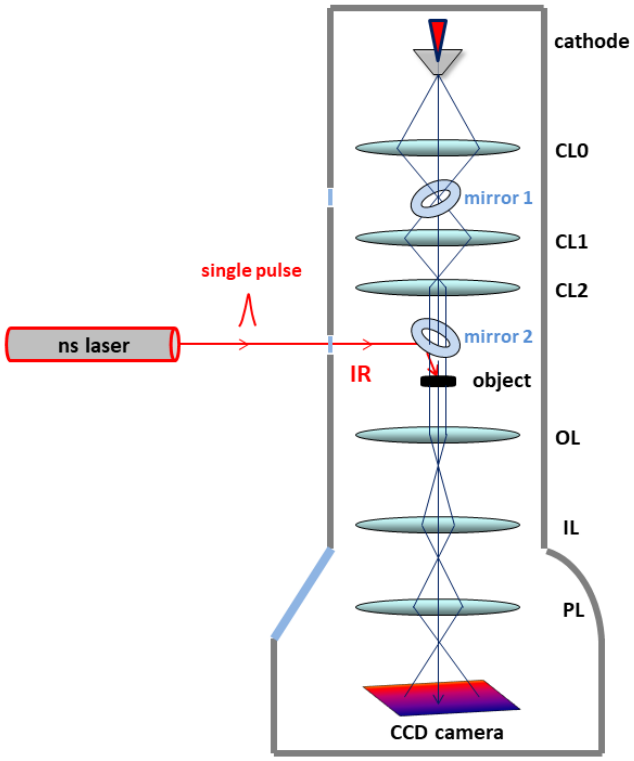

FIG. S1. Schematic drawing of the electron microscope with the nanosecond laser coupled to the microscope.

2. Electron irradiation effects in the specimen

The Ti_3O_5 crystals turned out to be sensitive to electron irradiation. A typical electron beam current density of 1 mA cm^{-2} on the specimen was used for imaging and diffraction to minimize radiation damage. Structural changes of the crystals started after approximately 30 minutes of irradiation under these low-dose conditions, corresponding to a critical dose of 10^3 e^- $Å^{-2}$ at an electron energy of 200 keV. This made the time-consuming tilting procedure and the diffraction measurements under slow temperature changes challenging. Lattice imaging normally needs beam current densities of the order 1 A cm^{-2} which would limit the beam exposure to a few seconds. This is insufficient for observing the phase transformation under slow heating.

Since Ti_3O_5 is semiconducting in the β-phase and metallic in the λ-phase, ionization and bond breaking effects should be less important than in insulators due to quenching of ionization by the conduction electrons. Nevertheless, considerable damage occurs which might not only be due to electronic excitations but also to ballistic displacements of oxygen atoms by the energetic electrons in the beam. Heating by the electron beam is generally low in TEM specimens, but since the crystals have thicknesses of up to almost 1 μm, some thermal influence cannot be excluded at higher electron beam intensity. This is another reason why a low intensity of the electron beam was used. Phase transformations induced by the electron beam were not observed before the crystals were amorphized (for a review of beam damage in oxides, see, e.g., N. Jiang*, Rep. Prog. Phys*. **2016**, *79*, 016502). Modern developments in high-speed data collection with fast-frame-rate electron detectors and dedicated specimen tilt procedures would allow a more efficient low-dose acquisition of diffraction patterns in 3D (see Y. Ling et al. *Nat. Commun*. **2022**, *13*, 6625).

3. Supplementary results

3.1 Thermal phase transformation

Figure S2 shows size changes of a Ti_3O_5 crystal upon heating. Since no diffraction information could be obtained in this case, the phases are given on the basis of the history and the temperature of the sample (initially beta, alpha at 623 K, lambda after cooling).

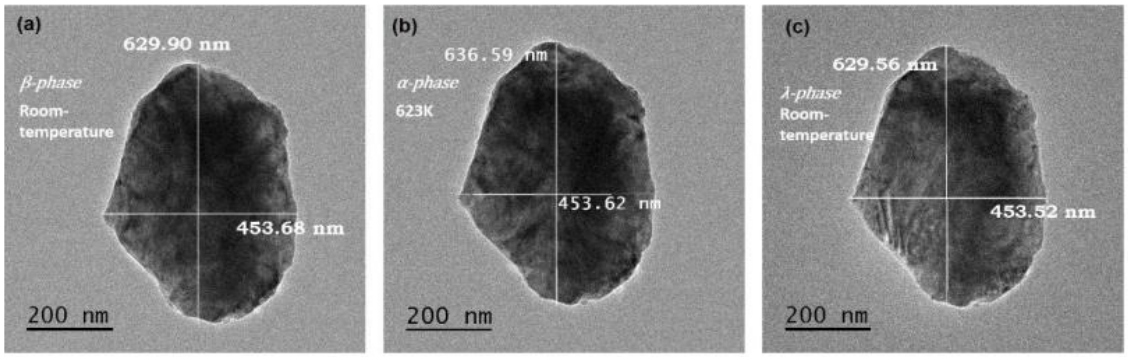

FIG. S2. Shape changes of a Ti_3O_5 crystal during a heating-cooling cycle. (a) Initial shape at room temperature; (b) at 623 K; (c) after cooling back to room temperature. Measurements of the sizes are indicated.

3.2. Laser-induced phase transformation

Figure S3 shows the laser-induced phase transformation but ion another crystal as shown in Fig. 4 of the main text.

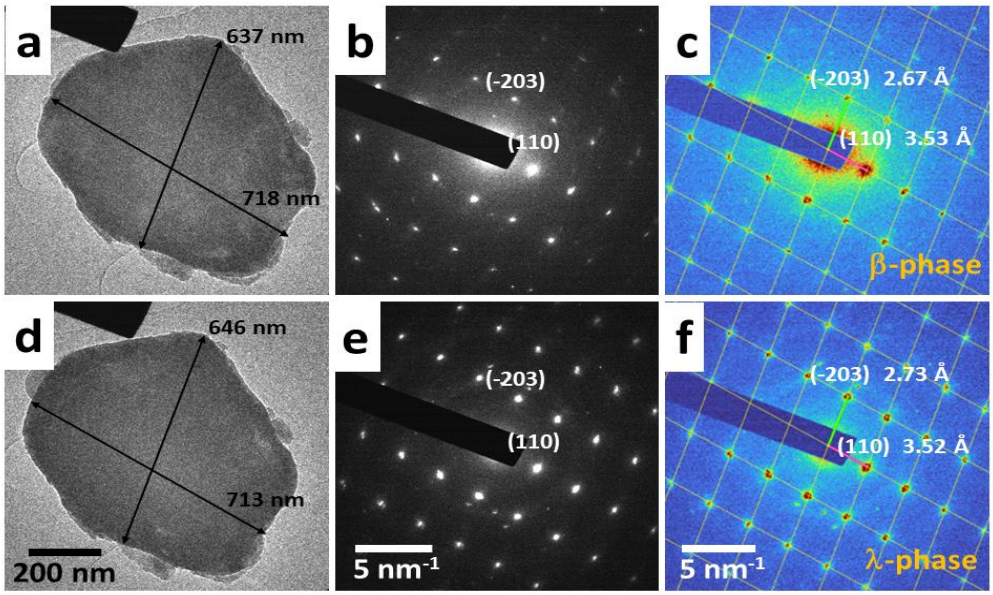

FIG. S3. Phase transformation under a single laser pulse. Images (a, d), diffraction patterns (b, e) and simulated diffraction patterns (c, f) of a Ti_3O_5 crystal. (a – c): β-phase before the transformation; (d – f): λ-phase after the transformation under a 7 ns laser pulse at 15 mJ/cm^2

and at 1064 nm. The measured dimensions of the particle and the spacings of the diffraction spots are indicated. The same directions for the measurements were chosen in diffraction and imaging. In (c) and (f), the experimental patters are overlaid with the calculated reciprocal lattice of the respective phase in the $[3\bar{3}2]$ zone axis (orange lines) which fits the experimental patterns.

	beta	**lambda**	**% change**
lattice spacings from diffraction in Å (in parentheses: from X-ray diffraction[1])			
(110)	3.53 (3.54)	2.52 (3.54)	±0% (±0%)
$(\bar{2}03)$	2.67 (2.68)	2.73 (2.72)	+2.2% (+1.5%)
size of the particle in nm			
(110)	718	713	-0.7%
$(\bar{2}03)$	637	646	+1.4% (

TABLE S1. Analysis of the diffraction patterns and images shown in Figure SI 2. The results from electron diffraction are compared with values from X-ray diffraction in the literature (in parentheses).

[1] I. E. Grey, C. Li, and I. C. Madsen, *J. Solid State Chem*. **1994**, *113*, 62.

4. Crystallographic data of Ti_3O_5

beta[1]:	9.757 Å	3.801 Å	9.439 Å	90.00°	91.55°	90.00°
lambda[1]:	9.826	3.789	9.969	90.00	90.56	90.00
changes $\beta \rightarrow \lambda$	+1.3%	+1%	+6.5%			
alpha[2]:	3.798	9.846	9.988	90.00	90.00	90.00

[1] I. E. Grey, C. Li, and I. C. Madsen, *J. Solid State Chem.* **1994**, *113*, 62.

[2] M. Onoda, *J. Solid State Chem.* **1998,** *136*, 67.

5. Electron diffraction pattern indexation

The indexation process of electron diffraction patterns consists in:

a. Raw estimation of diffraction pattern center and two basis vectors of the zeroth order Laue zone.
b. Least square refinement of center and basis vectors against positions of a list of selected centered diffraction peaks, distributed in the 2D-ZOLZ.
c. Look-up of possible (*hkl*) indexation of the two basis vectors according to a set of cell parameters corresponding to possible expected crystallographic phases, and within a fixed uncertainty range in both vectors' lengths and angle.
d. Selection of a possible indexation and least square refinement of the scale factor and azimuthal angle of the 2D lattice against all the selected experimental peaks.

In case several indexations are possible within the selected resolution, the retained one corresponds to the minimum of:

- root mean square distance from experimental peak positions to the model ones,
- minimum deviation of the scale factor compared to a reference indexation,
- minimum deviation of azimuthal angle between experimental and model lattices.

The diffraction peak centering is done using an iterative estimation of the intensity weighted average position of the peak within a square box of given size. At each step, the box is re-centered on the previous estimation and iteration is ran until convergence, within half a pixel size or fixed maximum number of iterations.

The whole process has been coded into Matlab® graphical interface "UTEMtoolkit", available upon request to philippe.rabiller@univ-rennes.fr *(MATLAB version: 9.12.0 (R2022a), Natick, Massachusetts: The MathWorks Inc.; 2022)*.

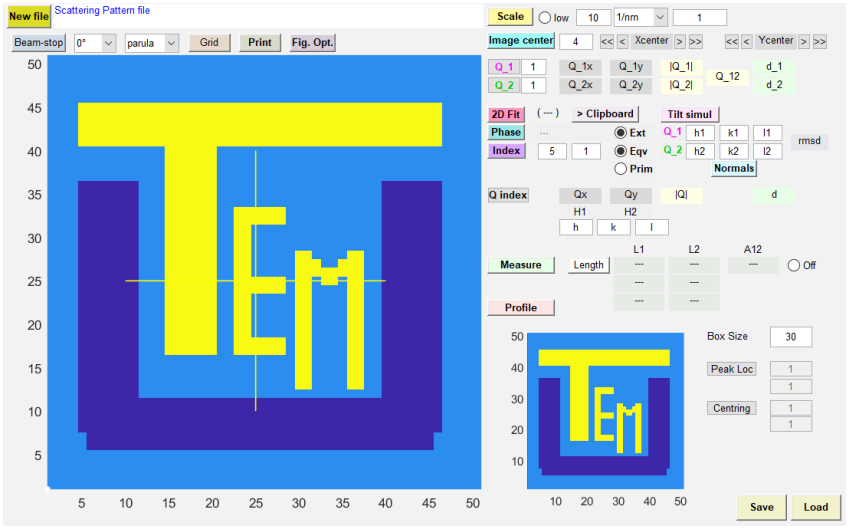

FIG. S4. Graphical interface designed for indexing TEM electron diffraction images.

6. Calculus of elongation from diffraction patterns

Direct space basis vectors $(\mathbf{d}_1, \mathbf{d}_2)$ can be computed from the two basis vectors $(\mathbf{q}_1, \mathbf{q}_2)$ of the zeroth order Laue zone (Fig. S5a), using the orthogonality rule: $d_\alpha \cdot q_\beta = \delta_{\alpha\beta}$

Cartesian coordinates $\mathrm{X} = (X_1, X_2)$ can be computed from fractional ones $\mathrm{x} = (x_1, x_2)$ as follows, introducing the transformation matrix D (see Fig. S5b):

$$X = \mathrm{x}\, D \qquad \text{with} \quad D = \begin{pmatrix} d_{11} & d_{12} \\ d_{12} & d_{22} \end{pmatrix}$$

Let X be the cartesian coordinates of a circle of unit radius ($|\mathrm{X}| = 1$), the fractional coordinates given in a basis linked to a phase "I" will be $\mathrm{x} = X_{II}\, D_{II}^{-1}$. If phase I transforms into phase II, the set fractional coordinates x corresponds to cartesian ones: $\mathrm{X}_{II} = \mathrm{x}\, D_{II} = \mathrm{X}_I\, D_I^{-1} D_{II}$ in phase II (Fig. S5c).

The relative elongation in polar coordinates: $\frac{\delta L(\theta)}{L} = 1 - |\mathrm{X}_{II}|(\theta)$ is plotted in Fig. S5d.

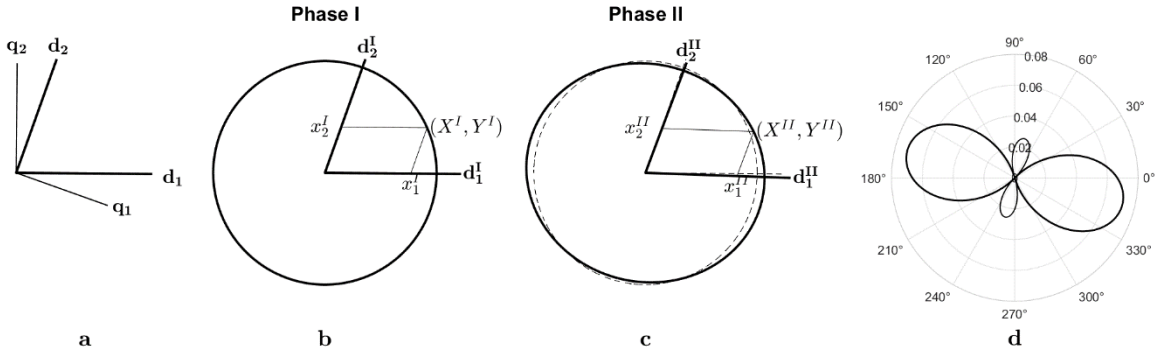

FIG. S5. Illustration of the relative elongation seen in plane of the zeroth order Laue zone (LZ0). a) Direct space vectors corresponding to the LZ0 basis vectors. b) Circular contour expressed in the phase I coordinates. c) deformation of the circular contour upon transition from phase I to phase II. c) relative elongation in polar coordinates.

7. Indexing of rings in the diffraction patterns of Figures 1e and 1f

In Figs. 1e and 1f, obtained after slow heating, extra spots appear, corresponding to misoriented and randomly aligned crystallites that lead to spots distributed along diffraction rings. An attempt of indexing of these rings has been done for Figs. 1e and 1f with the different phases' parameters. The indexing is shown in Figures S6 and S7. Bragg peak indexing based on the least square fit

procedure leads to a root mean square deviation of about 0.5 to 1 pixels. The shown model rings are within a distance of +/- 3 pixels apart from the selected observed rings. From Figs. S6 and S7, it seems that the observed rings most probably correspond to the beta-phase, indicating an incomplete transformation. One possible explanation could be that residual stress induced by ball-milling in the sample prevents from complete switching to the alpha and/or lambda phase upon heating, leading to a breaking of part of the sample into misoriented small crystallites. In Fig. 1f, corresponding to the longer exposure to the electron beam and full heating treatment, extra rings appear for which no proper indexing can be made within the resolution of +/3 pixels, indicating a possible degradation of the sample or transformation into another oxide of titanium.

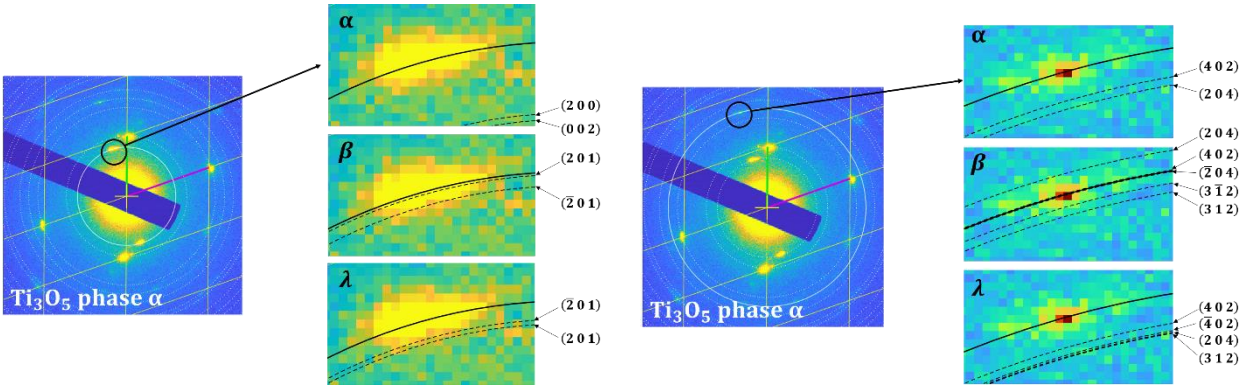

FIG. S6. Attempt of indexing the ring-like spots in Fig. 1e. A full line corresponds to the observed rings and dashed lines correspond to possible indexing in the phases alpha, beta or lambda. Left part: indexing of a ring with smaller diameter, right part: indexing of a ring with larger diameter.

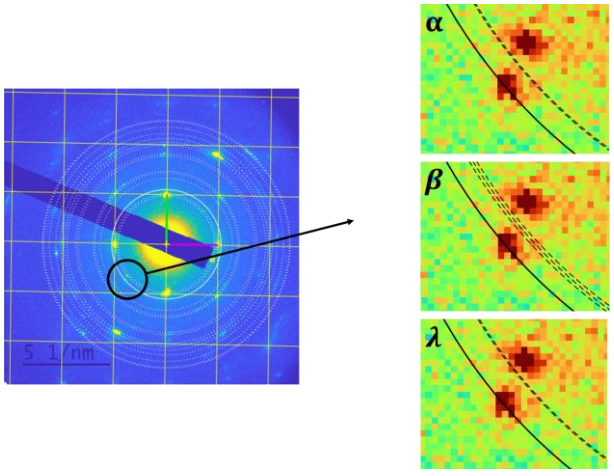

FIG. S7. Attempt of indexing of Fig. 1f for an extra ring not corresponding to possible phases of Ti_3O_5. The full line corresponds to the observed ring, the dashed lines correspond to closest possible indexing in the phases alpha, beta or lambda.

8. Estimation of the specimen heating under laser pulses

According to Yoshimatsu et al. (*Crystal Growth Design* **2021**, *22*, 703), the absorption at 1064 nm wavelength (1.15 eV) in 100 nm Ti_3O_5 films is 35%. The absorption is 100% - $T - R$ (T: transmission, R: reflection). This value is in satisfactory agreement with that obtained by Hakoe et al. (*Materials Letters*, **2017**, *188*, 8) using ellipsometry, also on a 100 nm thin film in the λ-phase (absorption coefficient at 1064 nm wavelength: 0.7 x 10^5 cm^{-1}). While those measurements were carried out for the λ-phase, Ohkoshi et al. (*Nature Chem.* **2010**, *2*, 539) have shown that in the vicinity of 1064 nm, the optical coefficients of the λ- and the β-phase are not too different.

The intensity loss is $I / I_0 = \exp(-\alpha t)$, where α is the absorption coefficient and t the thickness of the sample. Therefore, from Yoshimatsu et al., we can deduce $I / I_0 = 0.65$ at $t = 100$ nm, this gives $I / I_0 = 0.18$ at $t = 400$ nm, corresponding to 82 % absorption.

The laser power (energy Q / surface A) in this study is Q/A = 15 mJ cm^{-2} = 150 J m^{-2}. With 82% absorption, this leads to 0.82 x Q/A = 123 J m^{-2}

The heat is $Q = C\, m\, \Delta T$, where the specific heat is C = 160 J K^{-1} mol^{-1} = 7.1x10^2 J kg^{-1} K^{-1} (Tokoro et al., Nat. Comm. **2015**, *6,* 7037) and the density ρ = 4500 kg m^{-3}.

Then, we obtain $\Delta T = \frac{Q/A}{C\rho t}$ and for t = 400 nm: **$\underline{\Delta T = 96\ K}$**

For t = 300 nm, we would get ΔT = 122 K and for t = 500 nm ΔT = 84 K, so the temperature rise isn't dramatically changing with specimen thickness.

Of course, this is a rough estimate because

-The laser power could be higher if we are in the center of the Gaussian beam profile or lower if we are outside the waist of the FWHM. There is always a slight drift of the laser spot on the specimen due to the typical pointing instability of these lasers.

- Reflection losses at the particle surface should lead to somewhat less absorption but are difficult to estimate for the irregular surface of these particles.